International Journal of Pharmaceutics 410 (2011) 196–205

Contents lists available at ScienceDirect

International Journal of Pharmaceutics

journal homepage: www.elsevier.com/locate/ijpharm

Pharmaceutical nanotechnology

Molecular modeling of gel nanoparticles with cyclosporine A for oral drug delivery

Jonáš Tokarský[a,*], Tomáš Andrýsek[b], Pavla Čapková[a]

[a] Nanotechnology Centre, VŠB-Technical University of Ostrava, 17.listopadu 15, 708 33 Ostrava, Czech Republic
[b] Teva Czech Industries s.r.o., Ostravská 29, 747 70 Opava, Czech Republic

ARTICLE INFO

Article history:
Received 21 November 2010
Received in revised form 6 March 2011
Accepted 13 March 2011
Available online 21 March 2011

Keywords:
Cyclosporine A
Molecular modeling
Drug delivery
Structure characterization

ABSTRACT

Structure and behavior of amphiphilogel nanoparticles as a drug carriers for cyclosporine A (CsA) have been studied by the molecular modeling using empirical force field. Five atomistic models of a gel-based emulsions (GEM) with various gel compositions have been investigated in order to find a system most similar to a sixth atomistic model of self-microemulsifying drug delivery system (SMEDDS) taken as an exemplar of CsA delivery system. Structural parameters and energy characteristics (i.e. non-bond interaction energy between CsA and whole remaining components of a gel nanoparticle, CsA/gel nanoparticle intermolecular non-bond interaction energy, CsA–gel molecule pair interaction energy, volume fraction, concentration profiles and number of pervaded water molecules) of these six models in a waterless form and in a water containing form have been studied in dependence on the composition. The Flory–Huggins theory as implemented in the Accelrys Materials Studio 4.2 modeling environment was used to study the pair interactions of cyclosporine A with various types of surfactants. Structural parameters and energy characteristics of all systems have been compared and one composition was selected as a very promising for further experimental study.

1. Introduction

Cyclosporine A (CsA) as a powerful immunosuppressive agent exhibits very low aqueous solubility. This poor solubility led to the search for new formulations suitable for oral drug delivery. During decades two major concepts for final drug delivery were worked out. An older one, self-emulsifying drug delivery system (SEDDS), was used in post-transplant rejection treatment until the middle of the nineties of the last century, when it was replaced by another concept – so called self-microemulsyfying drug delivery system (SMEDDS) and self-nanoemulsyfying drug delivery system (SNEDDS) (Mueller et al., 1994; Kovarik et al., 1994; Rao and Shao, 2008). The main difference between those two concepts was observed in particle size distribution of created dispersion. While mean particle size of SEDDS was generally in micron range, mean particle size of SMEDDS were below 1 μm. Mean particle size of SNEDDS were about 50 nm (Andrýsek et al., 1998; Rao and Shao, 2008; Pouton, 1997). This difference in physico–chemical characteristic resulted from a change in composition, where besides new surfactant with hydrophilic–lipophylic balance higher then 10 the lipophylic component based on partial lipids were used as the drug carrier. All those changes led to the dramatic increase in bioavailability of CsA. Therefore, it has been assumed that the size of particles is an important factor in absorption of drug from these compositions. However, a bit later also formulations with the mean particle size higher than 1 μm based on the similar surfactants were discovered exploiting polyglycerol esters as the carrier components, which were able to deliver CsA into a body within the similar rate and extent as microemulsions (Andrýsek, 2001; Uhrikova et al., 2004; Murdan et al., 2005).

Because among the main characteristics of such systems belongs ability to create a mezophase in contact with the aqueous medium (e.g. lyotropic liquid crystalline phase) reminiscenting gel structure, they were called gel-based emulsions (GEM) (Andrýsek, 2001; Murdan et al., 2005).

To understand similarity and difference between SMEDDS and GEM systems several studies were initiated among which computer molecular modeling using empirical force field in *Accelrys Materials Studio 4.2* modeling environment was involved. The basis of molecular modeling is that all important molecular properties are related to the molecular structure. Structures we have to analyze in pharmacotechnology are usually too large for *ab initio* calculations. In such a case the molecular mechanics using empirical force field is the right tool for structure analysis and properties prediction due to a computational siplicity and efficiency. Molecular mechanics allows us to optimize the structure and bonding geometry by the total potential energy minimization, where the potential energy is described by the empirical force field (Comba and Hambley, 1995).

* Corresponding author. Tel.: +420 597 321 519, fax: +420 597 321 640.
E-mail address: jonas.tokarsky@vsb.cz (J. Tokarský).

0378-5173/$ – see front matter © 2011 Elsevier B.V. All rights reserved.
doi:10.1016/j.ijpharm.2011.03.026

Molecular modeling has also another advantage: it is much cheaper and less time consuming than real experimental studies in laboratory. From the large amount of possible gel compositions only the CsA/gel systems having promising properties are selected using molecular modeling. These selected mixtures can be further studied experimentally. Therefore, the presented work is not focused on using the molecular modeling for the detailed prediction of all properties of real systems. The aim was to use a simple parameters in order to find the models of GEM systems which are the most similar to the model of SMEDDS and to exclude the dissimilar systems.

In this work we compared the models of six systems containing various surfactants for oral CsA delivery: GEM systems (denoted as A, B, D–F) and SMEDDS (denoted as C). The effect of the composition on structure, shape and stability of nanoparticle containing CsA molecule was evaluated using structural parameters like radius of gyration, volume fraction, concentration profiles and energy characteristics: the non-bond interaction energy between CsA molecule and whole remaining components of a gel nanoparticle, CsA–gel component pair mixing energy and intermolecular non-bond interaction energy of CsA/gel nanoparticle. Attention has been paid also to the pervasion of water molecules into the CsA/gel nanoparticle. Strategy of molecular modeling, which has been worked out, is usable for any lipid-based drug carriers. Presented structural parameters and energy characteristics can be used for arbitrary composition and give us the possibility to compare various drug carriers in order to find the most suitable one.

2. Materials and methods

2.1. Compositions of the real samples

Compositions of the real samples are presented.

Sample A: CsA: 10 wt.%, cremophor RH 40 (Cr): 30 wt.%, decaglycerol monooleate (DGM): 20 wt.%, triglycerol monooleate (TGM): 30 wt.%, ethanol (Et): 10 wt.%.
Sample B: CsA: 10 wt.%, Cr: 50 wt.%, TGM: 30 wt.%, Et: 10 wt.%.
Sample C: CsA: 10 wt.%, Cr: 40 wt.%, glycerol monolinoleate (GML): 10 wt.%, glycerol dilinoleate (GDL): 20 wt.%, propylene glycol (PG): 10 wt.%, Et: 10 wt.%.
Sample D: CsA: 10 wt.%, Cr: 40 wt.%, TGM: 26 wt.%, polyethylene glycol (PEG): 10 wt.%, Et: 14 wt.%.
Sample E: CsA: 10 wt.%, Cr: 40 wt.%, TGM: 26 wt.%, diethylene glycol monoethyl ether (DEG): 10 wt.%, Et: 14 wt.%.
Sample F: CsA: 10 wt.%, Cr: 40 wt.%, TGM: 26 wt.%, Et: 14 wt.%, labrasol: 10 wt.%. labrasol itself is the mixture of three following compounds: polyethylene glycol-8-caprinate (PEGC): 50 wt.%, glycerol monocaprylate (GMC): 25 wt.%, glycerol dicaprylate (GDC): 25 wt.%. Therefore, sample F contains 5.0 wt.% of PEGC, 2.5 wt.% of GMC and 2.5 wt.% of GDC.

2.2. Preparation of the initial models

Series of six sample models denoted as A, B, C, D, E, F with various compositions has been prepared for molecular mechanics and molecular dynamics computations. Initial models with periodic boundary conditions have been built according to the compositions of six samples mentioned above. Number of molecules in the unit cell corresponds to the weight proportions of components in real sample. All models have been investigated in the waterless form (denoted as A0, B0, C0, D0, E0, F0) and in the water containing form with 60 wt.% of water (denoted as A60, B60, C60, D60, E60, F60).

Model of sample A: 1 CsA, 1 Cr, 2 DGM, 5 TGM and 19 Et molecules for A0 (i.e. 0 wt.% of water); resp. 1 CsA, 1 Cr, 2 DGM, 5 TGM, 19 Et and 764 water molecules for A60 (corresponding to 60 wt.% of water in the final mixture).
Model of sample B: 1 Cy, 2 Cr, 7 TGM and 26 Et molecules for B0; resp. 1 Cy, 2 Cr, 7 TGM, 26 Et and 944 water molecules for B60.
Model of sample C: 1 Cy, 2 Cr, 3 GML, 4 GDL, 16 PG and 26 Et molecules for C0; resp. 1 Cy, 2 Cr, 3 GML, 4 GDL, 16 PG, 26 Et and 1045 water molecules for C60.
Model of sample D: 1 Cy, 2 Cr, 7 TGM, 3 PEG and 41 Et molecules for D0; resp. 1 Cy, 2 Cr, 7 T, 3 PEG, 41 Et and 1104 water molecules for D60.
Model of sample E: 1 Cy, 2 Cr, 7 TGM, 10 DEG and 41 Et molecules for E0; resp. 1 Cy, 2 Cr, 7 T, 10 DEG, 41 Et and 1113 water molecules for E60.
Model of sample F: 1 Cy, 2 Cr, 7 TGM, 1 PEGC, 1 GMC, 1 GDC and 41 Et molecules for F0; resp. 1 Cy, 2 Cr, 7 TGM, 1 PEGC, 1 GMC, 1 GDC, 41 Et and 1091 water molecules for F60.

All these initial models have been prepared in the unit cells under the periodic boundary conditions. Structural formulae of the components of CsA/gel nanoparticles (CsA molecule, all surfactants, PG and Et) are reported in Fig. 1a–m.

For building the models of CsA/gel nanoparticles the Cr conformation with sixteen (8 + 8) oxyethylene units in both side chains and with eight (4 + 4) oxyethylene units in the middle chain has been chosen. While the real Cr is always a mixture of various conformations, for the modeling purpose only one conformation must be used because there is only one Cr molecule in models A and two Cr molecules in models B, C, D, E, F. Therefore, twelve different conformations have been prepared and optimized in order to find the conformation with the lowest total energy, i.e. the most stable and the most probable conformation. All these conformations fulfilled the condition that the sum of number of oxyethylene units (L + M + N + X + Y + Z, see Fig. 2) in the Cr molecular structure must be fourty. Table 1 shows the total energy values for the optimized conformations. Conformation L8M4N8X8Y4Z8 exhibiting the best, i.e. the lowest, total energy can be seen in the Fig. 1b.

2.3. Modeling conditions

Smart algorithm (i.e. the cascade of Steepest descent, Conjugate gradient and Quasi-Newton optimization algorithms) with 50,000 cycles was used for the geometry optimization of Cr conformations. Polymer consistent force field (*pcff*) (Maple et al., 1988) was used to parametrize atoms in the models. The convergence tresholds for the maximum energy and maximum force changes were 4.187×10^{-4} kJ/mol and 20.935×10^{-2} kJ/mol/nm, respectively. For the Coulombic and the van der Waals forces the atom based summation method was used **(citace)**. Atomic charges have been assigned by the *pcff*.

Models have been treated using a procedure including three following steps: initial geometry optimization, molecular dynamics run and final geometry optimization. Initial geometry optimization is always a preliminary treatment of the models before the dynamics, so it is only of medium quality. Therefore, the convergence tresholds were 8.374×10^{-3} kJ/mol and 20.935×10^{-1} kJ/mol/nm for the maximum energy and maximum force changes, respectively. The rest of conditions were the same as in the case of Cr conformations optimization. Subsequently the molecular dynamics has been carried out under the following conditions: temperature $T = 298.15$ K (Nosé thermostat was used (Nosé, 1984)) and pressure $p = 101{,}325$ Pa (Berendsen barostat was used (Berendsen et al., 1984)). Length of the dynamics trajectory was 250 ps. Final geometry optimization after the dynamic run was realized under the same conditions as the Cr conformations optimization.

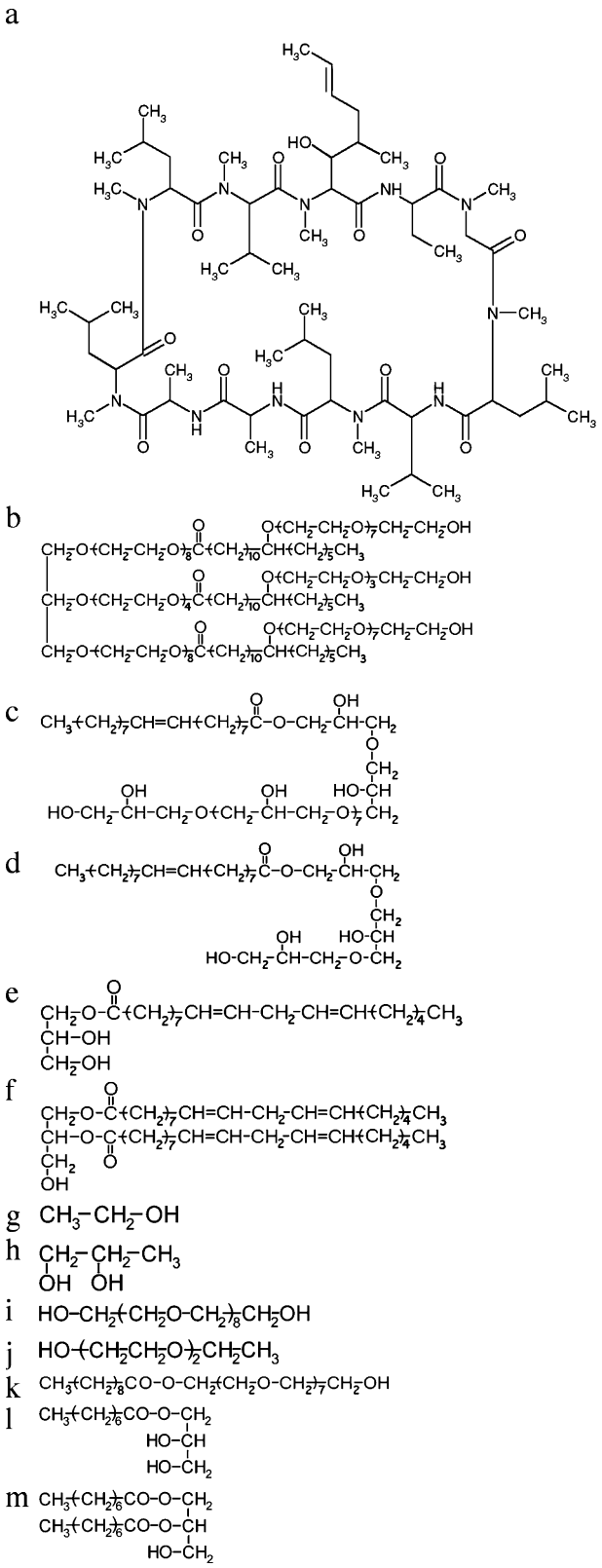

Fig. 1. (a) Structural formula of Cyclosporine A (CsA). (b) Structural formula of Cremophor RH 40 (Cr). (c) Structural formula of decaglycerol monooleate (DGM). (d) Structural formula of triglycerol monooleate (TGM). (e) Structural formula of glycerol monolinoleate (GML). (f) Structural formula of glyceriol dilinoleate (GDL). (g) Structural formula of ethanol (Et). (h) Structural formula of propylene glycol (PG). (i) Structural formula of polyethylene glycol (PEG). (j) Structural formula of diethylene glycol monoethyl ether (DEG). (k) Structural formula of polyethylene glycol-8-caprinate (PEGC). (l) Structural formula of glycerol monocaprylate (GMC). (m) Structural formula of glycerol dicaprylate (GDC).

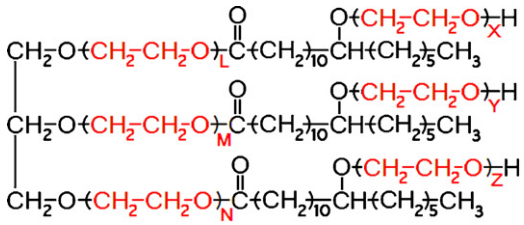

Fig. 2. Structure of Cremophor RH 40. Oxyethylene units are red and their numbers are represented by letters L, M, N, X, Y, Z.

2.4. Energy and structure characterizations

The non-bond interaction energy between CsA molecule and whole remaining components of a gel nanoparticle (E_{int}(CsA–gel)) and CsA/gel nanoparticle intermolecular non-bond interaction energy (E_{nb}) have been computed using the *pcff* in the *Accelrys Materials Studio – Forcite module*.

The non-bond interaction energy between CsA molecule and whole remaining components of a gel nanoparticle has been computed using following equation:

$$E_{int}(\text{CsA} - \text{gel}) = E_{tot}(\text{CsA/gel}) - (E_{tot}(\text{CsA}) + E_{tot}(\text{gel})) \quad (1)$$

where E_{tot}(CsA/gel) is the total potential energy of whole CsA/gel nanoparticle, E_{tot}(CsA) is the total potential energy of CsA molecule and E_{tot}(gel) is the total potential energy of all gel components.

Within the force field calculation, the total potential energy is described as a sum of the bonding and the non-bonding energy. Bonding energy describes the energy corresponding to the change of the bonding geometry, i.e. bond stretching, bond angle bending, torsion deformations etc. Non-bonding energy includes van der Waals, Coulombic and hydrogen interactions (Comba and Hambley, 1995).

E_{nb} was computed from the same optimized models as in case of Eq. (1) but the small molecules (Et for all models and in addition PG for models of C) and the water molecules (for the water containing models) were removed from the models. CsA/gel nanoparticle alone was obtained from the optimized model in this manner and its non-bond interaction energy (containing inter- and intramolecular contributions) was computed. The intramolecular contribution of non-bond interactions was excluded and as a result the E_{nb} holding the CsA and other molecules in gel nanoparticle together was obtained. Therefore, E_{nb} can be described using following equation:

$$E_{nb} = E_{nb}(\text{CsA/gel}) - \left(E_{nb}(\text{CsA}) + \sum_{i=1}^{n} E_{nb}(i^{\text{th}}\text{component}) \right) \quad (2)$$

where E_{nb}(CsA/gel) is the total non-bond energy of CsA/gel nanoparticle, E_{nb}(CsA) is the intramolecular non-bond energy of

Table 1
Values of the total energy for various conformations of the Cremophor RH 40 molecule revealed that the L4M8N4X4Y8Z4 conformation is the most probable one.

Cremophor RH 40 structure	Total energy (kJ/mol)
L8M4N8X8Y4Z8	−2010
L8M8N4X8Y8Z4	−1989
L5M10N5X5Y10Z5	−1980
L3M14N3X3Y14Z3	−1939
L5M5N10X5Y5Z10	−1897
L7M6N7X7Y6Z7	−1888
L7M7N6X7Y7Z6	−1880
L9M2N9X9Y2Z9	−1842
L3M3N14X3Y3Z14	−1834
L9M9N2X9Y9Z2	−1817
L1M1N18X1Y1Z18	−1788
L1M18N1X1Y18Z1	−1532

CsA molecule and E_{nb}(ith component) is the intermolecular energy of an ith component of the gel nanoparticle containing n components.

Pair interactions (i.e. the mixing energy) of components in mixtures characterizing the mutual solubility have been studied using Flory–Huggins theory (Flory, 1995). The general expression for the free energy of mixing in a binary system is:

$$\frac{\Delta G}{RT} = \frac{\Phi_b}{n_b}\ln\Phi_b + \frac{\Phi_s}{n_s}\ln\Phi_s + \chi\Phi_b\Phi_s \quad (3)$$

where ΔG is the free energy of mixing, Φ_b is the volume fraction of base, n_b is the degree of polymerization of base, Φ_s is the volume fraction of screen, n_s is the degree of polymerization of screen, χ is the interaction parameter, T is the absolute temperature and R is the gas constant. The first two terms in Eq. (3) describes the combinatorial entropy. This contribution, favoring a mixed state over the pure components, is negative. The third term is the free energy due to interaction.

Each component occupies a lattice site in the Flory–Huggins theory. For a lattice with coordination number Z the mixing energy (E_{mix}) is described by the expression:

$$E_{mix} = \frac{1}{2}Z(E_{bs} + E_{sb} - E_{bb} - E_{ss}) \quad (4)$$

where E_{bs}, E_{sb}, E_{bb} and E_{ss} are the binding energies and indexes b and s represent the base molecule and the screen molecule. One of the two molecules in a pair is always treated as a base during the pair interaction calculation. It means that this molecule is fixed and the second molecule (screen) takes various orientations against the base. A lot of pair configurations is generated during the calculation and binding energies have to be regarded as averages over an ensemble of this pair molecular configurations.

It must be noted that to calculate the compatibility of binary mixtures two extensions to the Flory–Huggins theory were employed (Blanco, 1991; Fan et al., 1992):

(a) Incorporating an explicit temperature dependence on the interaction parameter. This is accomplished by generating a large number of pair configurations and calculating the binding energies (as written before), followed by temperature averaging the results using the Boltzmann factor and calculating the temperature-dependent interaction parameter χ. It means that χ in Eq. (3) is equal to the E_{mix} divided by RT.
(b) Using an off-lattice calculation, meaning that molecules are not arranged on a regular lattice. The coordination number is calculated explicitly for each of the possible molecular pairs using molecular simulations.

Thus E_{mix} can be finally expressed as follows:

$$E_{mix} = \frac{1}{2}(Z_{bs}\langle E_{bs}\rangle_T + Z_{sb}\langle E_{sb}\rangle_T - Z\langle E_{bb}\rangle_T - E_{ss}\langle E_{ss}\rangle_T) \quad (5)$$

Small or negative value of E_{mix} indicates that at this particular temperature the two molecules have a favorable interaction (i.e. at given temperature the binary mixture shows one phase). If E_{mix} is large and positive, the molecules prefer to be surrounded by the same molecules rather than different ones and in this case the binary mixture will separate into two phases.

Pair interactions for all components in binary mixtures have been computed using *pcff*. Charges were also assigned by the *pcff*. The values of E_{mix} are summarized in Table 2. E_{mix} presented in Table 2 for each pair is the most frequent value for all combinations of two molecules. E_{mix} has been evaluated for 100,000 pair configurations.

In order to obtain quantitative characterization of optimized CsA/gel nanoparticles texture we introduced two following parameters for structure characterization: (a) the parameter φ (based on radius of gyration) and (b) the concentration profile.

Table 2
Pair interactions between CsA and all components of gel nanoparticles are listed. The highest solubility for CsA–DEG pair and the lowest solubility for CsA–PEGC pair can be seen.

Pairs	E_{mix} (kJ/mol)	Pairs	E_{mix} (kJ/mol)
CsA–DEG	−60.21	CsA–H_2O	−12.35
CsA–Cr	−44.59	CsA–TGM	−3.35
CsA–GDC	−33.33	CsA–Et	2.81
CsA–GMC	−32.99	CsA–DGM	11.81
CsA–GDL	−22.57	CsA–PEG	19.55
CsA–GML	−21.10	CsA–PEGC	80.43
CsA–PG	−16.25		

Table 3
Radii of gyration (R_g), unit cell volumes (V_{cell}) and volume fractions (φ) for all models including 60 wt.% of water are summarized in this table.

Models	R_g (nm)	V_{cell} (nm^3)	φ (%)
A60	1.24	34.4	23
B60	1.29	42.3	21
C60	1.41	47.1	25
D60	1.43	49.6	25
E60	1.49	50.1	28
F60	1.34	49.0	21

The radius of gyration (R_g) for one molecule has been computed from the following equation:

$$R_g = \sqrt{\frac{I}{M}} \quad (6)$$

where I is the moment of inertia of the molecule and M is the total mass of atoms in the molecule. R_g of whole CsA/gel nanoparticle can be computed in a same way. Then I is the moment of inertia of whole CsA/gel nanoparticle and M is the sum of mass of all atoms included in the CsA/gel nanoparticle.

For study of the behaviour of CsA/gel nanoparticle in water environment (whether it has a tendency to create the fibrous structure or not) the R_g value alone cannot be very helpful. The CsA/gel nanoparticles in the models A60, B60, C60, D60, E60 and F60 contain different number of molecules and so the R_g value is

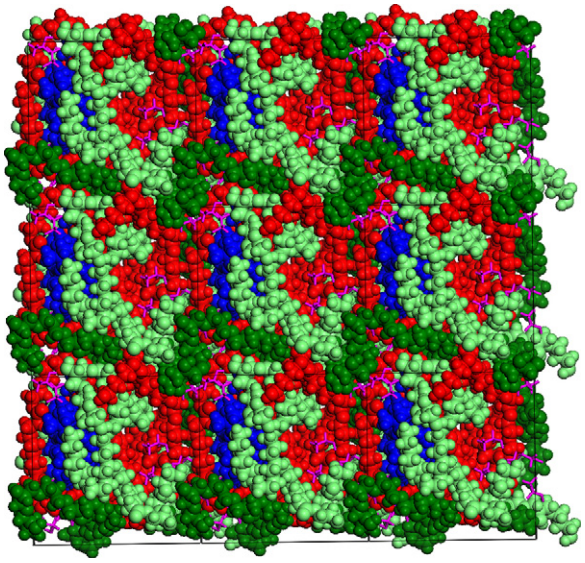

Fig. 3. Structure of optimized model A0 (i.e. containing 0 wt.% of water). Et molecules are displayed in the sticks mode. Colours: CsA-ultramarine, Cr-red, DGM-dark green, TGM-light green, Et-pink. For interpretation of the references to color in this figure legend, the reader is referred to the web version of the article.

influenced by the different size of CsA/gel nanoparticles. Therefore, it is impossible to compare the models in this way. For that reason the parameter φ (in principle the volume fraction of CsA/gel nanoparticle in the unit cell) was used.

The parameter φ is computed as follows:

$$\varphi = \frac{4/3\pi R_g^3}{V_{cell}} \times 100 \quad (7)$$

The numerator is an approximate volume of the CsA/gel nanoparticle (represented by the volume of sphere with radius equal to R_g of the CsA/gel nanoparticle). V_{cell} is a volume of the unit cell. It is evident that the more is the CsA/gel nanoparticle agglomerated (i.e. the less of volume occupies) the lower is φ. Although it is based on ideal assumptions (shapes of the CsA/gel nanoparticles are not really spherical) this parameter describes very well the structural changes which can be seen in Fig. 4a–f.

The values of R_g, V_{cell} and parameter φ are listed in Table 3.

Concentration profiles completing the informations obtained from volume fractions have been calculated by computing the profiles of atom density along each axis of the unit cell, i.e. parallel to the planes defined by (1 0 0), (0 1 0) and (0 0 1) vectors. This means simply taking the *x*, *y* nad *z* components of the fractional coordinates of each atom in the unit cell and generating the plot for each component independently. Each axis is divided equally into a number of bins. For plotting, the values of bins are converted from fractional positions to cartesian values. Charts displaying the concentration profiles can be seen in Fig. 5a–c for models A0, B0, C0 and Fig. 5d–f for models A60, B60, C60.

Values R_g and concentration profiles have been computed for the optimized models using *Accelrys Materials Studio–Forcite module* analysis tool.

3. Results and discussion

3.1. Pair interactions

Pair interactions between CsA and all components of gel mixtures have been computed using the Eq. (5). Values of E_{mix} (ordered according to the decreasing solubility) are summarized in Table 2. With the increasing value of E_{mix} the solubility decreases. The lowest value of E_{mix} (i.e. −60.21 kJ/mol for the CsA–DEG pair) shows the highest attractive interaction between these two molecules.

Table 2 shows that models B, C and E contain only gel molecules with the negative energy of mixing with CsA (i.e. the gel molecules having good miscibility with CsA). On the other hand in the models A, D and F there is always one molecule for which the energy of mixing with CsA is positive (DGM in case of A, PEG in case of D and PEGC in case of F).

3.2. Visual observation of the structures

One example of the optimized structure for the waterless sample A0 is presented in Fig. 3. All other waterless models look very similar, filling the unit cell completely.

Structures of optimized models A60–F60 (containing 60 wt.% of water) are displayed in the Fig. 4a–f. Atoms in CsA molecule and gel molecules are displayed as a spheres having van der Waals diameter. Because of the higher lucidity the small molecules of Et and PG are displayed in the stick mode and water molecules (the main part of unit cell content) are ommited. Comparing Figs. 4a–f one can see the differences between the models. While models A60 and B60 exhibit the tendency to create nearly isolated compact nanoparticles only with a slight mutual contact through the one molecule (Cr in case of A60, see Fig. 4a, and TGM in case of B60, see Fig. 4b), model C60 creates the nanoparticles with irregular and non-compact shape (see Fig. 4c). Samples D60, E60 and F60 exhibit the strong tendency to the fibrous structure as one can see in Fig. 4d–f.

3.3. Structure characterization of the models

In order to characterize the three-dimensional structures of the models in more details we used other characteristics such as parameter φ and concentration profiles.

Values of parameter φ (computed for all models using Eq. (7)) can be seen in Table 3. CsA/gel nanoparticles in models A60, B60 and F60 are more agglomerated than CsA/gel nanoparticles in models C60, D60 and E60. Comparing the values of parameter φ with Fig. 5a–f one can see that the models with less agglomerated CsA/gel nanoparticles (i.e. models C60, D60 and E60) have very irregular concentration profiles (the concentration profiles are discussed below). These three models has also the highest amount of pervaded water (see Table 6).

Concentration profiles in the three directions *x*, *y*, *z* are illustrated in Figs. 5a–f. For the computation of concentration profiles only the mass concentration of pure CsA/gel nanoparticles (i.e. containing CsA and gel molecules only) has been taken into account. Therefore, the optimized models have been modified in the following way.

The Et molecules have been removed from all models. Moreover, from the models C0 and C60 the PG molecules have been removed. In addition from the water containing models all water molecules have been removed.

Concentration profiles are in good agreement with conclusions derived from the Figs. 4a–f. Comparing the upper and lower charts in the Figs. 5a–f, one can see that the concentration profiles for all waterless samples are almost constant within the unit cell. The fact that there are no distinct concentration maxima indicates an entire filling of the unit cell by CsA/gel nanoparticles. The change of structure going from waterless sample to 60 wt.% of water can be seen in lower diagrams in Figs. 5a–f where the tendency to agglomeration is manifested by concentration maxima in the centre of the unit cell. Concentration profiles for the models A60 and B60 (see Fig. 5a and b) show nearly the same course for all three directions indicating the regular shape of CsA/gel nanoparticles. In case of C60 (see Fig. 5c) the irregular shape observed in the Fig. 4c manifests itself by the different shape of concentration profiles in *x*, *y* and *z* directions. For the models D60, E60 and F60 one can see in Figs. 5d–f that in some directions the concentration profiles are more flat within the unit cell and the relative concentration in these directions are higher near the border of the unit cells. These facts indicate the tendency to create the fibrous structure. For models D60 and F60 it is the one direction 010 (see Fig. 5d and f). In case of the model E60 these are two directions 1 0 0 and 0 0 1 (see Fig. 5e).

CsA/gel nanoparticles are larger in the models D60, E60 and F60 than in the models A60, B60 and C60. The largest CsA/gel nanoparticle is of E60 (see Fig. 5e). Moreover, the CsA/gel nanoparticles of models D60 and E60 are less agglomerated and more similar to the model C60 than CsA/gel nanoparticles in models A60, B60 and F60.

Visual observation of Figs. 5a–f can be extended by quantitative determination of the degree of agglomeration of CsA/gel nanoparticle. This quantitative determination is based on the following presumptions. It is evident that CsA/gel nanoparticle with atoms uniformly distributed throughout the volume of the unit cell will exhibit similar concentration profiles in each direction. If the concentration profiles are similar then the area delimited by curves of relative concentrations has a size equal to zero. The more irregular shape of CsA/gel nanoparticle (and the more disordered CsA/gel nanoparticle) the bigger difference between the concentration profiles in various directions. Further, it is evident that the bigger difference between the concentration profiles in various directions

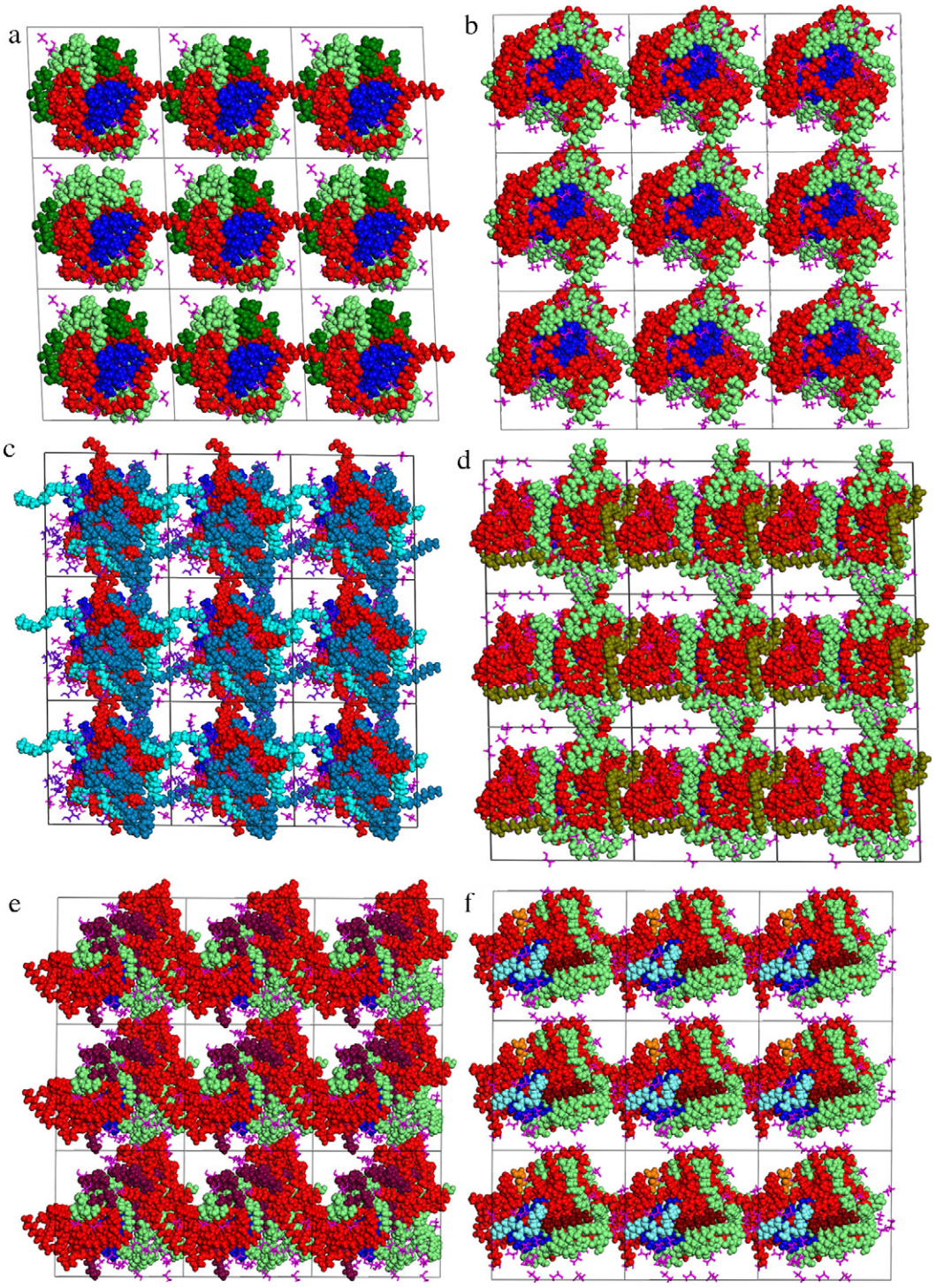

Fig. 4. (a) Structure of optimized model A60 (model containing 60 wt.% of water) in the projection into *XY* plane. Et molecules are displayed in the sticks mode. Colours: CsA-ultramarine, Cr-red, DGM-dark green, TGM-light green, Et-pink. For interpretation of the references to color in this figure legend, the reader is referred to the web version of the article. (b) Structure of optimized model B60 (model containing 60 wt.% of water) in the projection into *XZ* plane. Et molecules are displayed in the sticks mode. Colours: CsA-ultramarine, Cr-red, TGM-light green, Et-pink. For interpretation of the references to color in this figure legend, the reader is referred to the web version of the article. (c) Structure of optimized model C60 (model containing 60 wt.% of water) in the projection into *XZ* plane. Et and PG molecules are displayed in the sticks mode. Colours: CsA-ultramarine, Cr-red, GML-light blue, GDL-dark blue, Et-pink, PG-violet. For interpretation of the references to color in this figure legend, the reader is referred to the web version of the article. (d). Structure of optimized model D60 (model containing 60 wt.% of water) in the projection into *XY* plane. Et molecules are displayed in the sticks mode. Colours: CsA-ultramarine, Cr-red, TGM-light green, PEG-olive green, Et-pink. For interpretation of the references to color in this figure legend, the reader is referred to the web version of the article. (e) Structure of optimized model E60 (model containing 60 wt.% of water) in the projection into XZ plane. Et molecules are displayed in the sticks mode. Colours: CsA-ultramarine, Cr-red, TGM-light green, DEG-wine red, Et-pink. For interpretation of the references to color in this figure legend, the reader is referred to the web version of the article. (f) Structure of optimized model F60 (model containing 60 wt.% of water) in the projection into *YZ* plane. Et molecules are displayed in the sticks mode. Colours: CsA-ultramarine, Cr-red, TGM-light green, GMC-brown, GDC-ultralight blue, PEGC-orange, Et-pink. For interpretation of the references to color in this figure legend, the reader is referred to the web version of the article.

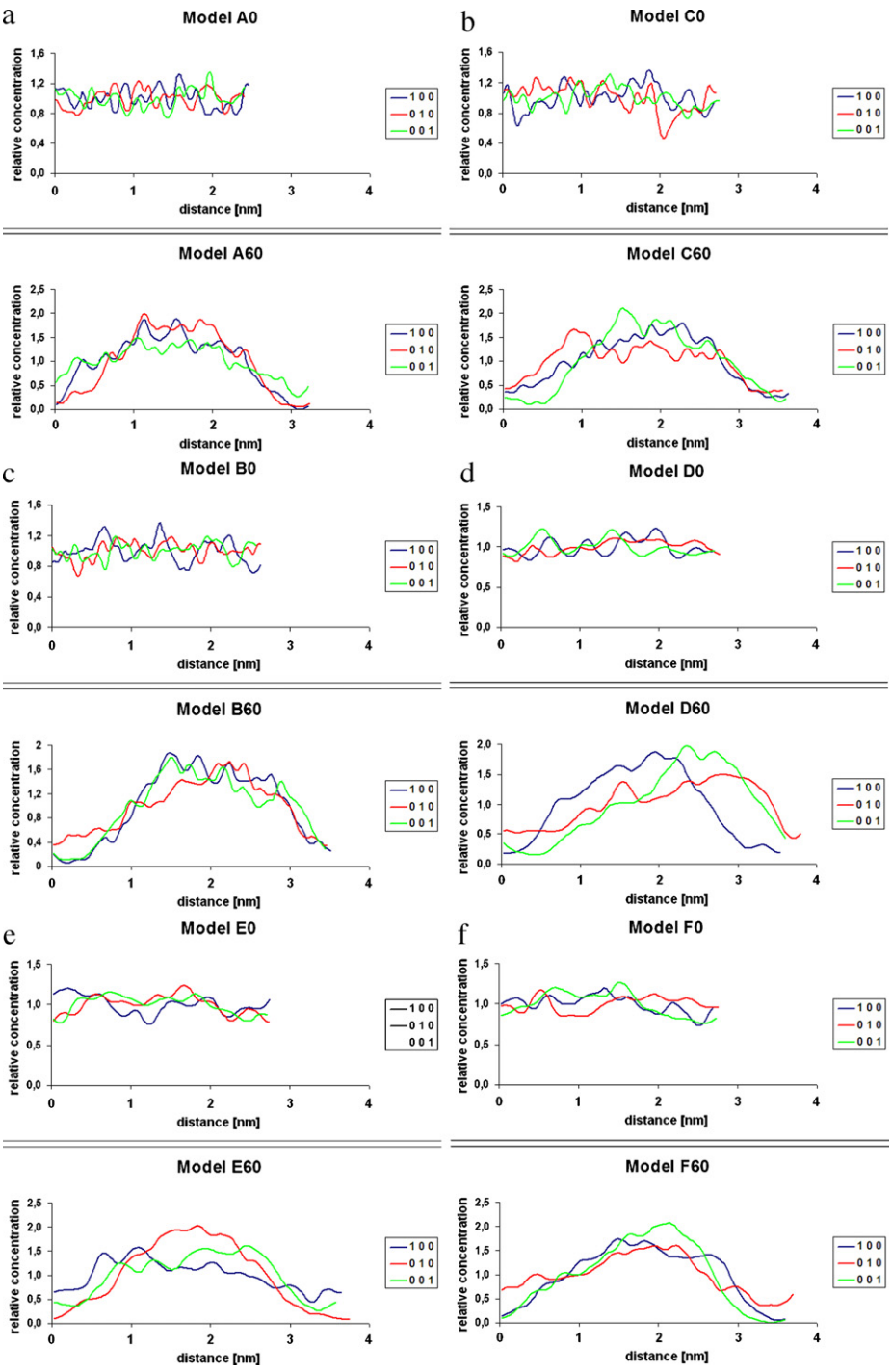

Fig. 5. (a) Concentration profiles of optimized models A0 (waterless model) and A60 (model containing 60 wt.% of water). Blue curve shows the relative concentration of atoms in the CsA/gel nanoparticle along the axis *x* (i.e. in 1 0 0 direction), red curve along the axis *y* (i.e. in 0 1 0 direction) and green curve along the axis *z* (i.e. in 0 0 1 direction). For interpretation of the references to color in this figure legend, the reader is referred to the web version of the article. (b) Concentration profiles of optimized models B0 (waterless model) and B60 (model containing 60 wt.% of water). Blue curve shows the relative concentration of atoms in the CsA/gel nanoparticle along the axis *x* (i.e. in 1 0 0 direction), red curve along the axis *y* (i.e. in 0 1 0 direction) and green curve along the axis *z* (i.e. in 0 0 1 direction). For interpretation of the references to color in this figure legend, the reader is referred to the web version of the article. (c) Concentration profiles of optimized models C0 (waterless model) and C60 (model containing 60 wt.% of water). Blue curve shows the relative concentration of atoms in the CsA/gel nanoparticle along the axis *x* (i.e. in 1 0 0 direction), red curve along the axis *y* (i.e. in 0 1 0 direction) and green curve along the axis *z* (i.e. in 0 0 1 direction). For interpretation of the references to color in this figure legend, the reader is referred to the web version of the article. (d) Concentration profiles of optimized models D0 (waterless model) and D60 (model containing 60 wt.% of water). Blue curve shows the relative concentration of atoms in the CsA/gel nanoparticle along the axis *x* (i.e. in 1 0 0 direction), red curve along the axis *y* (i.e. in 0 1 0 direction) and green curve along the axis *z* (i.e. in 0 0 1 direction). For interpretation of the references to color in this figure legend, the reader is referred to the web version of the article. (e) Concentration profiles of optimized models E0 (waterless model) and E60 (model containing 60 wt.% of water). Blue curve shows the relative concentration of atoms in the CsA/gel nanoparticle along the axis *x* (i.e. in 1 0 0 direction), red curve along the axis *y* (i.e. in 0 1 0 direction) and green curve along the axis *z* (i.e. in 0 0 1 direction). For interpretation of the references to color in this figure legend, the reader is referred to the web version of the article. (f). Concentration profiles of optimized models F0 (waterless model) and F60 (model containing 60 wt.% of water). Blue curve shows the relative concentration of atoms in the CsA/gel nanoparticle along the axis *x* (i.e. in 1 0 0 direction), red curve along the axis *y* (i.e. in 0 1 0 direction) and green curve along the axis *z* (i.e. in 0 0 1 direction). For interpretation of the references to color in this figure legend, the reader is referred to the web version of the article.

Table 4
Interaction energies between CsA molecule and whole remaining components of gel nanoparticle and total non-bond intermolecular interaction energies in CsA/gel nanoparticles per one atom for waterless models are listed.

Models	Number of atoms (*N*)	E_{int}(CsA–gel) (kJ/mol)	E_{nb}/N (kJ)
A0	1415	−942	−2.30
B0	1717	−934	−2.01
C0	1729	−1005	−1.55
D0	1915	−1080	−2.05
E0	1947	−1059	−2.01
F0	1902	−1089	−1.88

the bigger area delimited by curves of relative concentration. Therefore, the size of this area can be used as a parameter for quantitative determination of the degree of agglomeration of CsA/gel nanoparticle. Comparing the sizes of areas computed from the concentrations profiles of water containing models the degree of agglomeration of CsA/gel nanoparticles can be clearly seen: A60: 12.68, B60: 10.74, C60: 16.57, D60: 24.19, E60: 18.87, F60: 13.68. These values confirm the previous statements.

3.4. Energy characterization of the models

For the characterization of stability and cohesion energy of CsA/gel nanoparticles we introduced following parameters:

E_{int}(CsA–gel) (kJ/mol) is the interaction energy between CsA molecule and whole remaining components of a gel nanoparticle in the models A0–F0. This energy is not affected by the number of atoms in the CsA/gel nanoparticle.
E_{int60}(CsA–gel) (kJ/mol) is the interaction energy between CsA molecule and whole remaining components of a gel nanoparticle in the models A60–F60, where interactions with water molecules were omitted in the computations. This energy is not affected by the number of atoms in the CsA/gel nanoparticle.
E_{nb}/N (kJ) is the total non-bond intermolecular interaction energy in CsA/gel nanoparticles per one atom, characterizing the cohesion of whole nanoparticles.
E_{nb60}/N (kJ) is the total nonbond intermolecular interaction energy in CsA/gel nanoparticles per one atom, for the models A60–F60 characterizing the cohesion of whole CsA/gel nanoparticles. This energy has been calculated from the models after removing water molecules, so that interactions with water molecules were omitted in the computations.

The values of these parameters for all optimized models are listed in Table 4 (waterless models) and Table 5 (water containing models).

Comparing Table 4 and Table 5 it is evident that the presence of water significantly affects both E_{int}(CsA–gel) and E_{nb}/N which are higher (i.e. weaker) for the water containing models. This is related not only to the change of size and shape of CsA/gel nanoparticles in water environment (see the changes of concentraton profiles in Figs. 5a–f) but also to the pervasion of water (see Table 6 below).

Table 5
Interaction energies between CsA molecule and whole remaining components of gel nanoparticle and total non-bond intermolecular interaction energies in CsA/gel nanoparticles per one atom for water containing models are listed.

Models	Number of atoms (*N*)	E_{int60}(CsA–gel) (kJ/mol)	E_{nb60}/N (kJ)
A60	1415	−569	−0.30
B60	1717	−729	−0.29
C60	1729	−632	−0.24
D60	1915	−858	−0.28
E60	1947	−624	−0.28
F60	1902	−791	−0.28

Table 6
Total number of water molecules in the models and percentages of water molecules pervaded into the CsA/gel nanoparticles after the 250 ps of dynamics runs.

Models	Total number of water molecules	Pervaded water molecules (%)
A60	764	12.0
B60	944	12.7
C60	1045	19.2
D60	1104	16.6
E60	1113	16.9
F60	1191	7.5

Table 4 shows that values of E_{int}(CsA–gel) for models C0 and E0 are closer to each other than to the remaining models A0, B0, D0 and F0. The same result has been obtained in case of water containing models. In Table 5 it can be clearly seen that E_{int60}(CsA–gel) of C60 and E60 are nearly the same (−632 kJ/mol and −624 kJ/mol, respectively) while the values of E_{int60}(CsA–gel) for other models vary from −569 kJ/mol (A60) to −858 kJ/mol (D60).

E_{nb}/N and E_{nb60}/N parameters show the difference between GEM and SMEDDS. Models C0 and C60 exhibit the weakest cohesion (see Tables 4 and 5) which is in good agreement with the visual observations of the optimized models. Model C60 in Fig. 4c is much more irregular and less compact shaped than other optimized models in Fig. 4a and b, d–f. Thus the difference between the E_{nb60}/N for C60 and the E_{nb60}/N for other models illustrates the difference between the mean particle size of gel-based emulsion compositions and microemulsion compositions mentioned in the introduction.

3.5. Pervasion of water into the CsA/gel nanoparticle

Number of water molecules pervaded into the CsA/gel nanoparticle during the 250 ps of dynamics run is an important parameter. As mentioned before, E_{int}(CsA–gel) is affected by the pervasion of water. Total numbers of water molecules for all models containing water and percentages of pervaded water molecules are summarized in Table 6. Water molecule can be considered as pervaded only if the distance of this molecule from the geometrical mid-point of

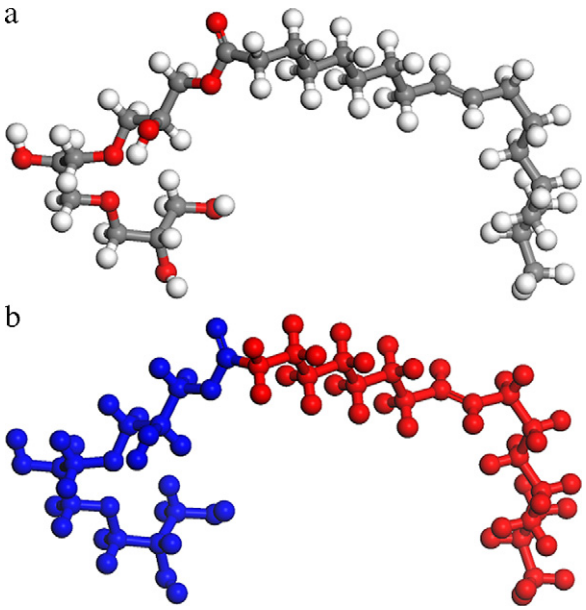

Fig. 6. (a) Molecule of triglycerol monooleate with distinct hydrophilic (glycerolic) and hydrophobic part of the chain. For interpretation of the references to color in this figure legend, the reader is referred to the web version of the article. (b) Molecule of triglycerol monooleate with coloured hydrophilic (blue) and hydrophobic (red) parts. For interpretation of the references to color in this figure legend, the reader is referred to the web version of the article.

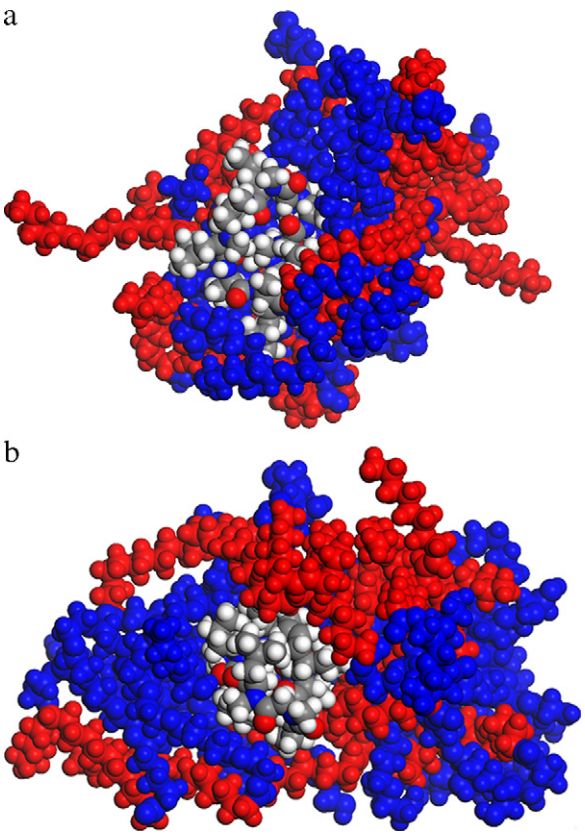

Fig. 7. (a) Hydrophilic (blue) and hydrophobic (red) parts of gel molecules in the model C60. Atoms in CsA molecule have the formal colours. For interpretation of the references to color in this figure legend, the reader is referred to the web version of the article. (b) Hydrophilic (blue) and hydrophobic (red) parts of gel molecules in the model E60. Atoms in CsA molecule have the formal colours. For interpretation of the references to color in this figure legend, the reader is referred to the web version of the article.

the CsA/gel nanoparticle is shorter than R_g of the CsA/gel nanoparticle. Table 6 shows the highest amount of pervaded water for the model C60 (19.2%). In the model E60 the 16.9% of water molecules are pervaded into the CsA/gel nanoparticle which is the closest to C60.

3.6. Hydrophilic and hydrophobic parts of molecules

Gel molecules in CsA/gel nanoparticles are either completely hydrophilic (Et, PG, DEG) or have the hydrophilic and hydrophobic parts (see Fig. 6a and b).

Therefore, the optimized models have been studied in order to answer a question whether the components of CsA/gel nanoparticles create a micelles in water environment. Hydrophilic parts of molecules were coloured blue, hydrophilic parts were coloured red and visual observations of optimized models led to the conclusion that CsA/gel nanoparticles do not create a micelles because there are no hydrophilic cover of a nanoparticle and no hydrophobic interior. Hydrophilic and hydrophobic parts of molecular chains are partially separated from each other but not in the direction from the mid-point of the nanoparticle to the surface. Two examples of such treated (coloured) CsA/gel nanoparticles can be seen in Fig. 7a (C60) and b (E60).

4. Conclusions

Molecular modeling using empirical force field has been used for the comparison of six systems for oral CsA delivery with various surfactants. Atomistic models of five GEM systems and one SMEDDS were investigated.

Six parameters characterizing the models were introduced: the interaction energy between CsA molecule and whole remaining components of a gel nanoparticle, the total non-bond intermolecular interaction energy in CsA/gel nanoparticles per one atom, CsA–gel molecule pair interaction energy, volume fraction of the CsA/gel nanoparticle in the unit cell, concentration profile and percentage of pervaded water molecules.

Presented results led to conclusions which can be briefly summarized in following notes:

(a) CsA/gel nanoparticles in models A60, B60 and F60 are more agglomerated than CsA/gel nanoparticles in models C60, D60 and E60.
(b) CsA/gel nanoparticles in models D, E and F exhibit the tendency to create fibrous structures in water environment.
(c) Interaction energy between CsA molecule and whole remaining components of a gel nanoparticle for models C and E are closer to each other than to the remaining models A, B, D and F.
(d) The percentage of pervaded water for model E60 is the closest to the percentage of pervaded water for model C60.
(e) Taking into account the results of pair interactions study the models C and E contain the gel molecules having very good miscibility with CsA molecule.
(f) CsA/gel nanoparticles do not create micelles in water environment.
(g) Results are consistent with each other.

GEM drug delivery system E is the most similar to the SMEDDS denoted as C and as such is very promising for further experimental study.

Our approach to the characterization of systems for oral drug delivery is simple and cheap. Presented structural parameters together with energy characteristics can be used (due to its universality) for arbitrary gel compositions in order to help the experimentalists find the most suitable GEM drug delivery systems.

Acknowledgement

This work was supported by the project of Ministry of Education in Czech Republic, project no: SP/2010140. Authors also wish to thank to Teva Czech Industries s.r.o. for supporting the research.

References

Andrýsek, T., 2001. The role of particle size distribution on bioavailability of Cyclosporine: novel drug delivery system. Biomed. Papers 145, 3–8.
Andrýsek, T., Vrána, A., Stuchlík, M., 1998. The effect of particle size on bioavailability for cyclosporine preparations based on the formation of submicron dispersions. Eur. J. Pharm. Sci. 8, S 77.
Berendsen, H.J.C., Postma, J.P.M., van Gunsteren, W.F., DiNola, A., Haak, J.R., 1984. Molecular dynamics with coupling to an external bath. J. Chem. Phys. 81, 3684–3690.
Blanco, M., 1991. Molecular silverware. I. General solutions to excluded volume constrained problems. J. Comput. Chem. 12, 237–247.
Comba, P., Hambley, T.W., 1995. Molecular Modeling of Inorganic Compounds, Second, completely revised and enlarged ed. Wiley-VCH, Weinheim, 17–56.
Fan, C.F., Olafson, B.D., Blanco, M., Hsu, S.L., 1992. Application of molecular simulation to derive phase diagrams of binary mixtures. Macromolecules 25, 3667–3676.
Flory, P.J., 1995. Principles of Polymer Chemistry, 16th printing. Cornell Univ. Press, Ithaca, NY, 507–511.
Kovarik, J.M., Mueller, F.A., van Bree, J.B., Tetzloff, W., Kutz, K., 1994. Reduced inter- and intraindividual variability in cyclosporine pharmacokinetics from a microemulsion formulation. J. Pharm. Sci. 83, 444–446.
Maple, J.R., Dinur, U., Hagler, A.T., 1988. Derivation of force fields for molecular mechanics and dynamics from *ab initio* energy surfaces. PNAS 85, 5350–5354.

Mueller, F.A., Kovarik, J.M., van Bree, J.B., Tetzloff, W., Grevel, J., Kutz, K., 1994. Improved dose linearity of cyclosporine pharmacokinetics from a microemulsion formulation. Pharm. Res. 11, 301–304.
Murdan, S., Andrýsek, T., Son, D., 2005. Novel gels and their dispersions – oral drug delivery systems for ciclosporin. Int. J. Pharm. 300, 113–124.
Nosé, S., 1984. A molecular-dynamics method for simulations in the canonical ensemble. Mol. Phys. 53, 255–268.
Pouton, C.W., 1997. Formulation of self-emulsifying drug delivery systems. Adv. Drug Del. Rev. 25, 47–58.
Rao, S.V.R., Shao, J., 2008. Self-nanoemulsifying drug delivery systems (SNEDDS) for oral delivery of protein drugs I. Formulation development. Int. J. Pharm. 362, 2–9.
Uhrikova, D., Andrýsek, T., Funari, S., Balgovy, P., 2004. Synchrotron radiation small- and wide-angle scattering study of dispergation of Equoral, a novel drug delivery system with cyclosporine A. Die Pharmazie 59, 650–651.